Supplement of Clim. Past, 16, 555–573, 2020
https://doi.org/10.5194/cp-16-555-2020-supplement

Climate of the Past
Open Access
EGU

Supplement of

Changes in the high-latitude Southern Hemisphere through the Eocene–Oligocene transition: a model–data comparison

Alan T. Kennedy-Asser et al.

Correspondence to: Alan T. Kennedy-Asser (alan.kennedy@bristol.ac.uk)

S1 Introduction

This supplementary information gives an overview of the three temperature datasets compiled for the late Eocene absolute temperatures, early Oligocene absolute temperatures and relative change in temperatures across the EOT (Section S2). Additionally, it provides some further information on the model simulation pairs used to simulate change across the EOT (Section S3) as well as examples of how the error between model and proxy data is calculated for the RMSE metrics (Section S4). Finally, it includes supplementary figures for the seasonal analysis referenced in the main text (Section S5) and full references for all of the data used in the compilations.

S2 Datasets

A full digital version of each dataset is available from the Open Science Framework (Kennedy-Asser, 2019).

Table S1: Compilation of temperature proxy records for the late Eocene.

Site	Palaeo-Lat.	Palaeo-Long.	Mean annual temp. (MAT; °C)	Max. MAT (°C)	Min. MAT (°C)	Proxy description	Age max. (Ma)	Age min. (Ma)	Source
Maud Rise	-65.3	1.6	12.3	13.3	11.3	Clumped isotopes	35.3	34.2	Value from Petersen & Schrag, 2015 (Table 2)
Prydz Bay	-66.2	73.0		12.0		Veg. NLR	39.0	34.0	Maximum value given in Trusswell & Macphail, 2009 (p. 100)
Prydz Bay	-66.2	73.0	10.3	13.9	6.7	S-index	35.8	33.7	Value from Passchier et al., 2016 (supp. info.), error from main text (p. 2)
Prydz Bay	-66.2	73.0		10.0		Dinocysts	35.4	33.6	Value from Houben et al., 2013, (Figure 3) and Zonnefeld et al., 2013 (Figure 208)
Kerguelen Plateau	-58.6	79.8	14.3	15.3	13.3	Mg/Ca	35.3	34.2	Offset from Maud Rise by 2°C, value in Bohaty et al., 2012, (Section 4.1)
Wilkes Land U1356	-61.1	130.3				No data			
Wilkes Land U1360	-66.3	136.8				No data			
S. Australia	-54.4	144.8	17.0	20.0	14.0	Veg. NLR	35.0	34.0	Korasidis et al. 2019 temperature estimate for T0 coal seam (mean between max. and min. range). Age is approximate based on Fig. 6.
S. Australia (region)	-54.4	144.8	16.0	20.6	11.3	Veg. Coexist.	36.6	34.0	Max. and min. values quoted in Pound & Salzmann, 2017 (p.4), location assumed the same as Korasidis et al.; mean taken between the max. and min. may be unrealistic
East Tasman Plateau	-60.7	152.9	22.4	24.9	19.9	TEX_{86}	37.0	33.7	Values from Houben et al. 2019 supplementary information (Molecular Paleothermometry tab). Mean is average of $TEX_{86}H$ calibration for values with BIT index <0.4 and depth 360-367.5 mbsf. Calibration error is taken as 2.5 from main text (p. 2218).

East Tasman Plateau	-60.7	152.9		10.0		Dinocysts	35.5	33.7	Value from Houben et al., 2013, (Figure 3) and Zonnefeld et al., 2013 (Figure 208)
Ross Sea	-76.7	155.9		13.0		Veg. NLR	41.0	34.0	Value from Francis et al., 2009 (p.333), location assumed the same as CRP-3 and age assumed 41-34 Ma (Bartonian/Priabonian)
Ross Sea	-76.7	155.9	8.7	12.3	5.1	S-index	36.2	34.2	Value from Passchier et al., 2013 (supp. info.; MAT sheet), error from main text (p. 1403)
New Zealand	-59.4	176.6	25.9	27.1	24.7	TEX_{86}	35.4	33.6	Value and error from Liu et al., 2009 (supp. info.), error of 2 stan. dev.
New Zealand	-59.4	176.6	25.6	27.6	23.6	$U^{K'}_{37}$	35.4	33.6	Value and error from Liu et al., 2009 (supp. info.), error of 2 stan. dev.
King George Isl.	-63.8	-62.6	10.0	15.0	5.0	Veg. NLR	41.0	34.0	Max. value from Birkenmajer & Zastawniak, 1989, main text (p. 238), date from main text (p. 234, discussion of loc. 7); Min. value from Francis et al. 2009 (p.330-331); mean taken between the max. and min. may be unrealistic
Seymour Isl.	-66.3	-58.4	12.8	16.0	9.2	Clumped isotopes	37.5	34.0	Value from Douglas et al., 2014 (supp. info., Table S3: mean of 34, 37.4 and 37.5 Ma values for both *Cucullaea* and *Eurhomalea*), error from maximum range of these values with their external error
Seymour Isl.	-66.3	-58.4	11.6	17.0	9.0	TEX_{86}	37.5	34.0	Value from Douglas et al., 2014 (supp. info., Table S4: mean of 34, 37.4 and 37.4 Ma TEX86L and TEX86' values), error from main text (p.4)
Seymour Isl.	-66.3	-58.4	16.5	22.3	10.7	MBT-CBT	37.5	34.0	Values from Douglas et al., 2014, (supp. info., Table S4: mean of 34, 37.4 and 37.5 Ma values). Two calibrations give very different values, taken here as a max. and min. range; mean (of max. and min.) may therefore be unrealistic
Weddell Sea	-64.0	-40.7		10.0		Dinocysts	36.6	33.6	Value from Houben et al., 2013, (Figure 3) and Zonnefeld et al., 2013 (Figure 208)
Falklands Plateau	-53.1	-38.6	18.4	22.0	14.8	TEX_{86}	37.1	33.3	Value and error from Liu et al., 2009 (supp. info.), error of 2 stan. dev.
Falklands Plateau	-53.1	-38.6	18.1	20.6	15.6	TEX_{86}	37.0	34.0	Values from Houben et al. 2019 supplementary information (Molecular Paleothermometry tab). Mean is average of $TEX_{86}H$ calibration for values with BIT index <0.4 and depth 138-180 mbsf

									(depth-ages taken from Liu et al. 2009 supp. info.). Calibration error is taken as 2.5 from main text (p. 2218).
Falklands Plateau	-53.1	-38.6	19.5	23.7	15.3	$U^{K'}_{37}$	37.1	33.3	Value and error from Liu et al., 2009 (supp. info.), error of 2 stan. dev.
S.W. Atlantic (region)	-60.0	-60.0	15.9	18.4	13.4	Veg. Coexist.	37.0	34.0	Max. and min. values quoted in Pound & Salzmann, 2017 (p.5), location is very large/unspecified, mean taken between the max. and min. may be unrealistic

15

Table S2: Compilation of temperature proxy records for the early Oligocene.

Site	Palaeo-Lat.	Palaeo-Long.	Mean annual temp. (MAT; °C)	Max. MAT (°C)	Min. MAT (°C)	Proxy description	Age max. (Ma)	Age min. (Ma)	Source
Maud Rise	-65.3	1.6	11.9	12.2	11.6	Clumped isotopes	33.0	31.9	Value from Petersen & Schrag, 2015 (Table 2)
Prydz Bay	-66.2	73.0	8.0	11.6	4.4	S-index	33.7	32.9	Value from Passchier et al., 2016 (supp. info.), error from main text (p. 2)
Prydz Bay	-66.2	73.0		10.0		Dinocysts	33.6	33.3	Value from Houben et al., 2013, (Figure 3) and Zonnefeld et al., 2013 (Figure 208)
Kerguelen Plateau	-58.6	79.8	11.7	13.5	9.9	Mg/Ca	34.0	33.2	Value from Bohaty et al., section 4.2, taken away from inferred late Eocene temp.; max. and min. allowing for error in absolute values (from Petersen & Schrag 2015) and change (Bohaty et al., 2012)
Wilkes Land U1356	-61.1	130.3	8.9	12.5	5.3	S-index	33.6	30.0	Value from Passchier et al. 2013 supp. info. (MAT sheet), error from main text (p. 1403)
Wilkes Land U1356	-61.1	130.3		10.0		Dinocysts	33.5	30.5	Value from Houben et al. 2013 figure 3 and Zonnefeld et al. 2013 figure 208
Wilkes Land U1356	-61.1	130.3	17.5	21.5	13.5	TEX_{86}	33.1	32.9	Value from Hartman et al. 2018 (reading first three points in record shown in Figure 3), with 4°C calibration error based on main text (p. 1285)
Wilkes Land U1360	-66.3	136.8		10.0		Dinocysts	33.6	32.4	Value from Houben et al. 2013 figure 3 and Zonnefeld et al. 2013 figure 208
S. Australia	-54.4	144.8	12.0	14.0	10.0	Veg. NLR	30.0	29.0	Korasidis et al. 2019 temperature estimate for M2A coal seam (mean

									between max. and min. range). Age is approximate based on Fig. 6.
S. Australia (region)	-54.4	144.8	16.0	20.6	11.3	Veg. Coexist.	33.0	30.0	Max. and min. values quoted in Pound & Salzmann, 2017 (p.4), location assumed the same as Korasidis et al. data; mean taken between the max. and min. may be unrealistic
East Tasman Plateau	-60.7	152.9	22.4	24.9	19.9	TEX_{86}	33.7	30.0	Values from Houben et al. 2019 supplementary information (Molecular Paleothermometry tab). Mean is average of $TEX_{86}H$ calibration for values with BIT index <0.4 and depth 358-360
Ross Sea	-76.7	155.9		10.0		Dinocysts	32.5	31.0	Value from Houben et al. 2013 figure 3 and Zonnefeld et al. 2013 figure 208
Ross Sea	-76.7	155.9	7.8	11.4	4.2	S-index	33.6	33.0	Value from Passchier et al., 2013 (supp. info.; MAT sheet), error from main text (p. 1403)
Ross Sea	-76.7	155.9	-2.0	8.0	-12.0	Vegetation NLR	32.0	31.0	Max. value from Passchier et al. 2013 supp. info. (vegetation sheet), based on their interpretation of similar modern ecosystem. Minimum value based on interpretations of Francis & Hill 1996. Approx. age from Prebble et al. 2006
New Zealand	-59.4	176.6	23.8	24.8	22.8	TEX_{86}	33.6	33.4	Value and error from Liu et al., 2009 (supp. info.), error of 2 stan. dev.
New Zealand	-59.4	176.6	22.4	23.8	21.0	$U^{K'}_{37}$	33.6	33.4	Value and error from Liu et al., 2009 (supp. info.), error of 2 stan. dev.
King George Isl.	-63.8	-62.6				No data			
Seymour Isl.	-66.3	-58.4				No data			
Weddell Sea	-64.0	-40.7		10.0		Dinocysts	33.6	33.2	Value from Houben et al., 2013, (Figure 3) and Zonnefeld et al., 2013 (Figure 208)
Falklands Plateau	-53.1	-38.6	11.2	14.4	8.0	TEX_{86}	33.7	33.1	Value and error from Liu et al., 2009 (supp. info.), error of 2 stan. dev.
Falklands Plateau	-53.1	-38.6	16.0	18.5	13.5	TEX_{86}	33.7	32.0	Values from Houben et al. 2019 supplementary information (Molecular Paleothermometry tab). Mean is average of $TEX_{86}H$ calibration for values with BIT index <0.4 and depth 20-130 mbsf (depth-ages taken from Liu et al. 2009 supp. info.). Calibration error is taken as 2.5 from main text (p. 2218).

Falklands Plateau	-53.1	-38.6	11.1	13.7	8.5	$U^{K'}_{37}$	33.7	33.1	Value and error from Liu et al., 2009 (supp. info.), error of 2 stan. dev.
S.W. Atlantic (region)	-60.0	-60.0	17.6	23.4	11.7	Veg. Coexist.	31.1	30.9	Max. and min. values quoted in Pound & Salzmann, 2017 (p.5), location is very large/unspecified, mean taken between the max. and min. may be unrealistic

20 **Table S3: Compilation of temperature proxy records across the Eocene-Oligocene Transition.**

Site	Palaeo-Lat.	Palaeo-Long.	Mean temp. change (°C)	Max. temp. change (°C)	Min. temp. change (°C)	Proxy description	Source
Maud Rise	-65.3	1.6			0.0	Nannofossils	General cooling suggested from Villa et al., 2013 (Figures 5 and 6)
Maud Rise	-65.3	1.6			0.0	Mg/Ca	General cooling suggested from Bohaty et al., 2012 (Figure 4b)
Maud Rise	-65.3	1.6	-0.4	-1.5	0.7	Clumped isotopes	Value from Petersen & Schrag, 2015 (Table 2)
Prydz Bay	-66.2	73.0			0.0	Dinocysts	*S. antarctica* increase shown in Houben et al., 2013 (Figure 3 and in supplementary dataset)
Prydz Bay	-66.2	73.0	-2.3	-5.1	0.5	S-index	Mean from difference in Passchier et al., 2016 (supp. info.); range taken from difference between max. and min. of each period based on 2 stan. dev.
Kerguelen Plateau	-58.6	79.8	-2.6	-3.4	-1.8	Mg/Ca	Value from Bohaty et al. 2012, section 4.2
Kerguelen Plateau	-58.6	79.8			0.0	Mg/Ca	General trend from Villa et al. 2013, Figure 2, 3 + 4
Wilkes Land U1356	-61.1	130.3				No data	
Wilkes Land U1360	-66.3	136.8				No data	
S. Australia	-54.4	144.8	-5.0	-10.0	0.0	Veg. NLR	Korasidis et al. 2019, Fig. 6 shows cooling, but with a relatively large gap in time between sections. Uncertainty range from difference in max. and min. values around each mean
S. Australia (region)	-54.4	144.8				Veg. Coexist.	Max. and min. values quoted in Pound & Salzmann 2017 (p.4) suggest a dip in MATR before the EOT, rising again to same values after; location assumed the same as Korasidis et al. data; mean taken between the max. and min. may be unrealistic

East Tasman Plateau	-60.7	152.9	0.0	-3.0	3.0	TEX_{86}	Values from Houben et al. 2019 supplementary information (Molecular Paleothermometry tab), TEX86H calibration. Uncertainty range from difference in max. and min. based on 2 SD around each mean. Houben et al. 2019 Fig. 3 shows record is very noisy.
Ross Sea	-76.7	155.9	-1.0	-5.9	4.0	S-index	Value from difference in Passchier et al. 2013 supp. info. (MAT sheet), error taken from extremes of each period calculated with 2 SD
Ross Sea	-76.7	155.9			0.0	Vegetation NLR	Vegetation reconstructions from multiple sources suggest cooler conditions in Oligocene, but estimates of by how much vary significantly
New Zealand	-59.4	176.6	-2.1	-2.9	-1.3	TEX_{86}	Value and error from Liu et al., 2009 (supp. info.)
New Zealand	-59.4	176.6	-3.1	-4.4	-1.8	$U^{K'}_{37}$	Value and error from Liu et al., 2009 (supp. info.)
King George Isl.	-63.8	-62.6				No data	
Seymour Isl.	-66.3	-58.4				No data	
Weddell Sea	-64.0	-40.7			0.0	Dinocysts	Increase shown in Houben et al. 2013 Figure 3 and in supplementary dataset
Falklands Plateau	-53.1	-38.6	-7.2	-9.6	-4.8	TEX_{86}	Value and error from Liu et al., 2009 (supp. info.)
Falklands Plateau	-53.1	-38.6	-2.1	-7.0	2.8	TEX_{86}	Values from Houben et al. 2019 supplementary information (Molecular Paleothermometry tab), TEX86H calibration. Uncertainty range from difference in max. and min. based on 2 SD around each mean
Falklands Plateau	-53.1	-38.6	-8.4	-10.9	-5.9	$U^{K'}_{37}$	Value and error from Liu et al., 2009 (supp. info.)
S.W. Atlantic (region)	-60.0	-60.0				Veg. Coexist.	Max. and min. values quoted in Pound & Salzmann, 2017 (p.5) suggest a dip in MATR before the EOT, rising again after to have wider range; location unclear

25

S3 Model simulation pairs

The model simulations used here have been previously described in Kennedy-Asser et al. (2019) and Ladant et al. (2014). Outlined here in Table S4 are the pairs of model simulations that make up each forcing scenario of the change across the EOT, as used in the model evaluation (Section 3.4). The output data from the HadCM3BL simulations can be freely accessed at: https://www.paleo.bristol.ac.uk/ummodel/scripts/papers/.

Table S4: Model simulation pairings used to represent various forcings across the Eocene-Oligocene Transition.

Model	Description as in Figure 5	Eocene setup (*simulation name*)	Oligocene setup (*simulation name*)
		AIS growth	
HadCM3BL	3x pCO_2, closed DP (EAIS)	AIS: none. *p*CO_2: 840 ppmv. Drake Passage: closed. (*tecqu2*)	AIS: EAIS. *p*CO_2: 840 ppmv. Drake Passage: closed. (*tecqt3*)
HadCM3BL	3x pCO_2, open DP (EAIS)	AIS: none. *p*CO_2: 840 ppmv. Drake Passage: open. (*tecqv1*)	AIS: EAIS. *p*CO_2: 840 ppmv. Drake Passage: open. (*tecqs1*)
HadCM3BL	2x pCO_2, closed DP (EAIS)	AIS: none. *p*CO_2: 560 ppmv. Drake Passage: closed. (*tecqp2*)	AIS: EAIS. *p*CO_2: 560 ppmv. Drake Passage: closed. (*tecqo2*)
HadCM3BL	2x pCO_2, open DP (EAIS)	AIS: none. *p*CO_2: 560 ppmv. Drake Passage: open. (*tecqq1*)	AIS: EAIS. *p*CO_2: 560 ppmv. Drake Passage: open. (*tecqn1*)
FOAM	2x pCO_2, warm orbit (small EAIS)	AIS: none. *p*CO_2: 560 ppmv. Drake Passage: open. (*FOAM.34Ma.WAM.2x.WSO*)	AIS: small EAIS. *p*CO_2: 560 ppmv. Drake Passage: open. (*FOAM.34Ma.WAM.2x.WSO.ISS1*)
FOAM	2x pCO_2, warm orbit (EAIS)	AIS: none. *p*CO_2: 560 ppmv. Drake Passage: open. (*FOAM.34Ma.WAM.2x.WSO*)	AIS: EAIS. *p*CO_2: 560 ppmv. Drake Passage: open. (*FOAM.34Ma.WAM.2x.WSO.ISS2*)
FOAM	2x pCO_2, warm orbit (full AIS)	AIS: none. *p*CO_2: 560 ppmv. Drake Passage: open. (*FOAM.34Ma.WAM.2x.WSO*)	AIS: full AIS. *p*CO_2: 560 ppmv. Drake Passage: open. (*FOAM.34Ma.WAM.2x.WSO.ISS3*)
FOAM	2x pCO_2, cold orbit (small EAIS)	AIS: none. *p*CO_2: 560 ppmv. Drake Passage: open. (*FOAM.34Ma.WAM.2x.CSO*)	AIS: small EAIS. *p*CO_2: 560 ppmv. Drake Passage: open. (*FOAM.34Ma.WAM.2x.CSO.ISS1*)

FOAM	2x pCO_2, cold orbit (EAIS)	AIS: none. pCO_2: 560 ppmv. Drake Passage: open. (*FOAM.34Ma.WAM.2x.CSO*)	AIS: EAIS. pCO_2: 560 ppmv. Drake Passage: open. (*FOAM.34Ma.WAM.2x.CSO.ISS2*)
FOAM	2x pCO_2, cold orbit (full AIS)	AIS: none. pCO_2: 560 ppmv. Drake Passage: open. (*FOAM.34Ma.WAM.2x.CSO*)	AIS: full AIS. pCO_2: 560 ppmv. Drake Passage: open. (*FOAM.34Ma.WAM.2x.CSO.ISS3*)
		AIS growth + pCO_2 drop	
HadCM3BL	Closed DP (EAIS, 3x-2x pCO_2)	AIS: none. pCO_2: 840 ppmv. Drake Passage: closed. (*tecqu2*)	AIS: EAIS. pCO_2: 560 ppmv. Drake Passage: closed. (*tecqo2*)
HadCM3BL	Open DP (EAIS, 3x-2x pCO_2)	AIS: none. pCO_2: 840 ppmv. Drake Passage: open. (*tecqv1*)	AIS: EAIS. pCO_2: 560 ppmv. Drake Passage: open. (*tecqn1*)
FOAM	Warm orbit (small EAIS + 3x-2x)	AIS: none. pCO_2: 840 ppmv. Drake Passage: open. (*FOAM.34Ma.WAM.3x.WSO*)	AIS: small EAIS. pCO_2: 560 ppmv. Drake Passage: open. (*FOAM.34Ma.WAM.2x.WSO.ISS1*)
FOAM	Warm orbit (EAIS + 3x-2x)	AIS: none. pCO_2: 840 ppmv. Drake Passage: open. (*FOAM.34Ma.WAM.3x.WSO*)	AIS: EAIS. pCO_2: 560 ppmv. Drake Passage: open. (*FOAM.34Ma.WAM.2x.WSO.ISS2*)
FOAM	Warm orbit (full AIS + 3x-2x)	AIS: none. pCO_2: 840 ppmv. Drake Passage: open. (*FOAM.34Ma.WAM.3x.WSO*)	AIS: full AIS. pCO_2: 560 ppmv. Drake Passage: open. (*FOAM.34Ma.WAM.2x.WSO.ISS3*)
FOAM	Warm orbit (small EAIS + 4x-2x)	AIS: none. pCO_2: 1,120 ppmv. Drake Passage: open. (*FOAM.34Ma.WAM.4x.WSO*)	AIS: small EAIS. pCO_2: 560 ppmv. Drake Passage: open. (*FOAM.34Ma.WAM.2x.WSO.ISS1*)
FOAM	Warm orbit (EAIS + 4x-2x)	AIS: none. pCO_2: 1,120 ppmv. Drake Passage: open. (*FOAM.34Ma.WAM.4x.WSO*)	AIS: EAIS. pCO_2: 560 ppmv. Drake Passage: open. (*FOAM.34Ma.WAM.2x.WSO.ISS2*)
FOAM	Warm orbit (full AIS + 4x-2x)	AIS: none. pCO_2: 1,120 ppmv. Drake Passage: open. (*FOAM.34Ma.WAM.4x.WSO*)	AIS: full AIS. pCO_2: 560 ppmv. Drake Passage: open. (*FOAM.34Ma.WAM.2x.WSO.ISS3*)
FOAM	Cold orbit (small EAIS + 3x-2x)	AIS: none. pCO_2: 840 ppmv. Drake Passage: open. (*FOAM.34Ma.WAM.3x.CSO*)	AIS: small EAIS. pCO_2: 560 ppmv. Drake Passage: open. (*FOAM.34Ma.WAM.2x.CSO.ISS1*)
FOAM	Cold orbit (EAIS + 3x-2x)	AIS: none. pCO_2: 840 ppmv. Drake Passage: open. (*FOAM.34Ma.WAM.3x.CSO*)	AIS: EAIS. pCO_2: 560 ppmv. Drake Passage: open. (*FOAM.34Ma.WAM.2x.CSO.ISS2*)

FOAM	Cold orbit (full AIS + 3x-2x)	AIS: none. pCO_2: 840 ppmv. Drake Passage: open. (*FOAM.34Ma.WAM.3x.CSO*)	AIS: full AIS. pCO_2: 560 ppmv. Drake Passage: open. (*FOAM.34Ma.WAM.2x.CSO.ISS3*)
FOAM	Cold orbit (small EAIS + 4x-2x)	AIS: none. pCO_2: 1,120 ppmv. Drake Passage: open. (*FOAM.34Ma.WAM.4x.CSO*)	AIS: small EAIS. pCO_2: 560 ppmv. Drake Passage: open. (*FOAM.34Ma.WAM.2x.CSO.ISS1*)
FOAM	Cold orbit (EAIS + 4x-2x)	AIS: none. pCO_2: 1,120 ppmv. Drake Passage: open. (*FOAM.34Ma.WAM.4x.CSO*)	AIS: EAIS. pCO_2: 560 ppmv. Drake Passage: open. (*FOAM.34Ma.WAM.2x.CSO.ISS2*)
FOAM	Cold orbit (full AIS + 4x-2x)	AIS: none. pCO_2: 1,120 ppmv. Drake Passage: open. (*FOAM.34Ma.WAM.4x.CSO*)	AIS: full AIS. pCO_2: 560 ppmv. Drake Passage: open. (*FOAM.34Ma.WAM.2x.CSO.ISS3*)
		AIS growth + DP opening	
HadCM3BL	3x pCO_2 (EAIS, DP opening)	AIS: none. pCO_2: 840 ppmv. Drake Passage: closed. (*tecqu2*)	AIS: EAIS. pCO_2: 840 ppmv. Drake Passage: open. (*tecqs1*)
HadCM3BL	2x pCO_2 (EAIS, DP opening)	AIS: none. pCO_2: 560 ppmv. Drake Passage: closed. (*tecqp2*)	AIS: EAIS. pCO_2: 560 ppmv. Drake Passage: open. (*tecqn1*)
		All	
HadCM3BL	(EAIS, 3x-2x pCO_2, DP opening)	AIS: none. pCO_2: 840 ppmv. Drake Passage: closed. (*tecqu2*)	AIS: EAIS. pCO_2: 560 ppmv. Drake Passage: open. (*tecqn1*)

S4 Error calculation

As discussed in Section 2.4, for the model-data comparison, the error, E, between the modelled temperature, T_m, and proxy reconstructed temperature, T_p, for a given site and time period, i, is taken between the limits of the uncertainty range from both the modelled and the proxy reconstructed temperatures. If there is any overlap between the uncertainty ranges, E is taken as 0. For proxy records that provide an upper limit to the temperature, if the lower limit from the model is less than the proxy upper limit, E is taken as 0; otherwise E is taken as the difference between the model lower limit and the proxy. Examples of how this is calculated are illustrated in Figure S1.

The error can be calculated in this way for the standard RMSE metric ($E_{S,i}$) using the raw values of temperature from the datasets or model simulations, or for the normalised RMSE metric ($E_{N,i}$) if the mean temperature of all proxy data points/sites is removed from the datasets and simulation data.

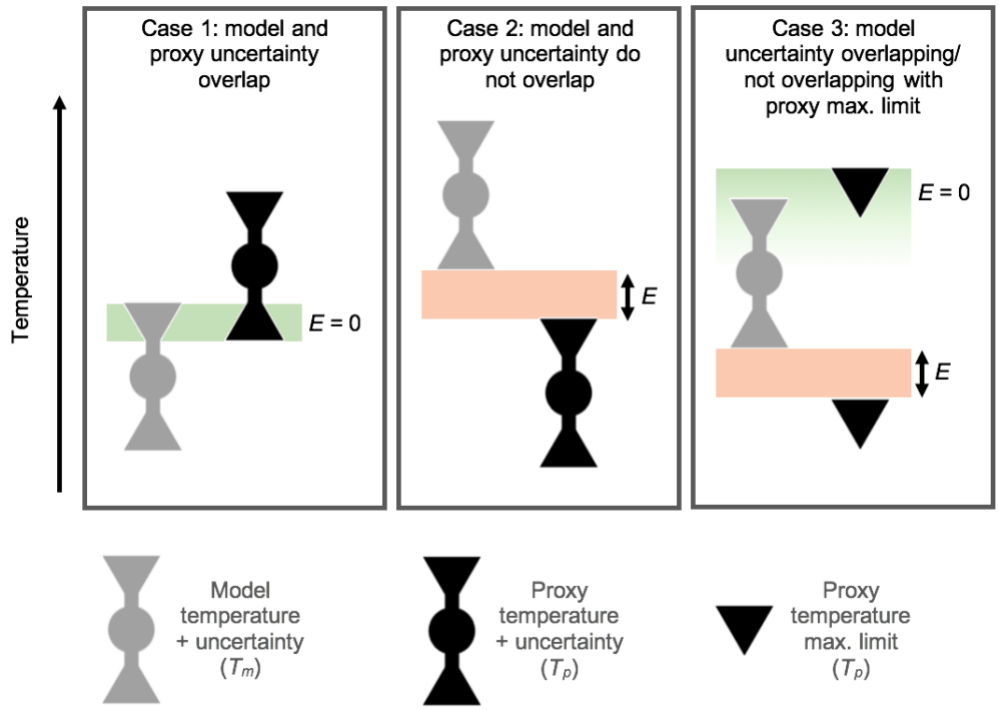

Figure S1: examples of how the error, *E*, is calculated for the standard and normalise RMSE metrics.

S5 Supplementary figures for seasonal analysis

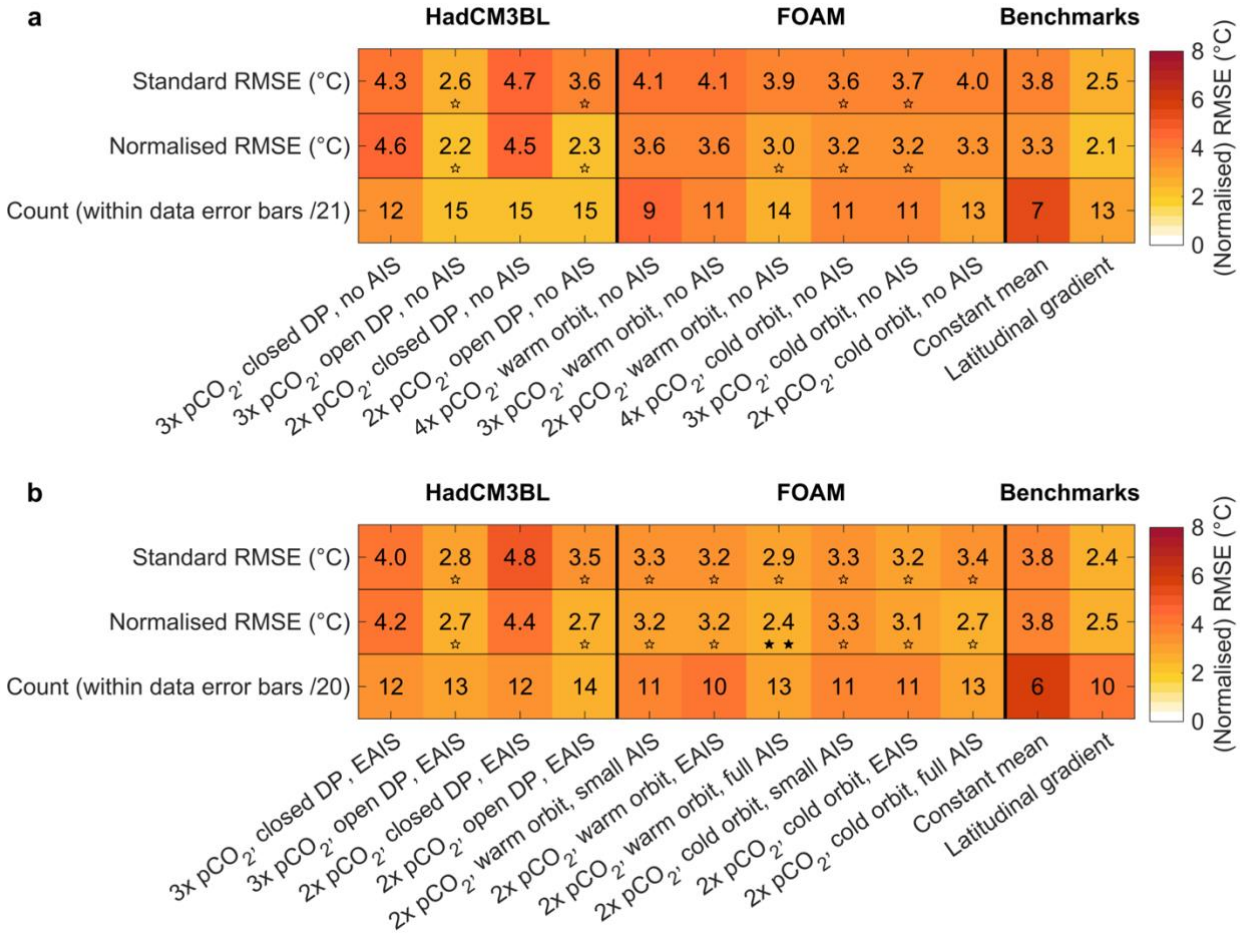

Supplementary Figure 2: Standard RMSE (°C), normalised RMSE (°C) and count metric for the summer (DJF) mean temperature from all model simulations and the benchmarks compared against the late Eocene dataset (a) and the early Oligocene dataset (b). Labels on the x-axis refer to the pCO_2 level ('2x', '3x' or '4x' pre-industrial levels), state of the Drake Passage ('DP') in HadCM3BL simulations and the size of the Antarctic ice sheet (AIS). The colour scale of the count metric is normalised to match that of the RMSE metrics (i.e. white = best: all sites are within error bars; dark orange = worst: no sites are within error bars). For a given metric, single open stars indicate simulations with *moderate* performance and double black stars indicate simulations with *good* performance.

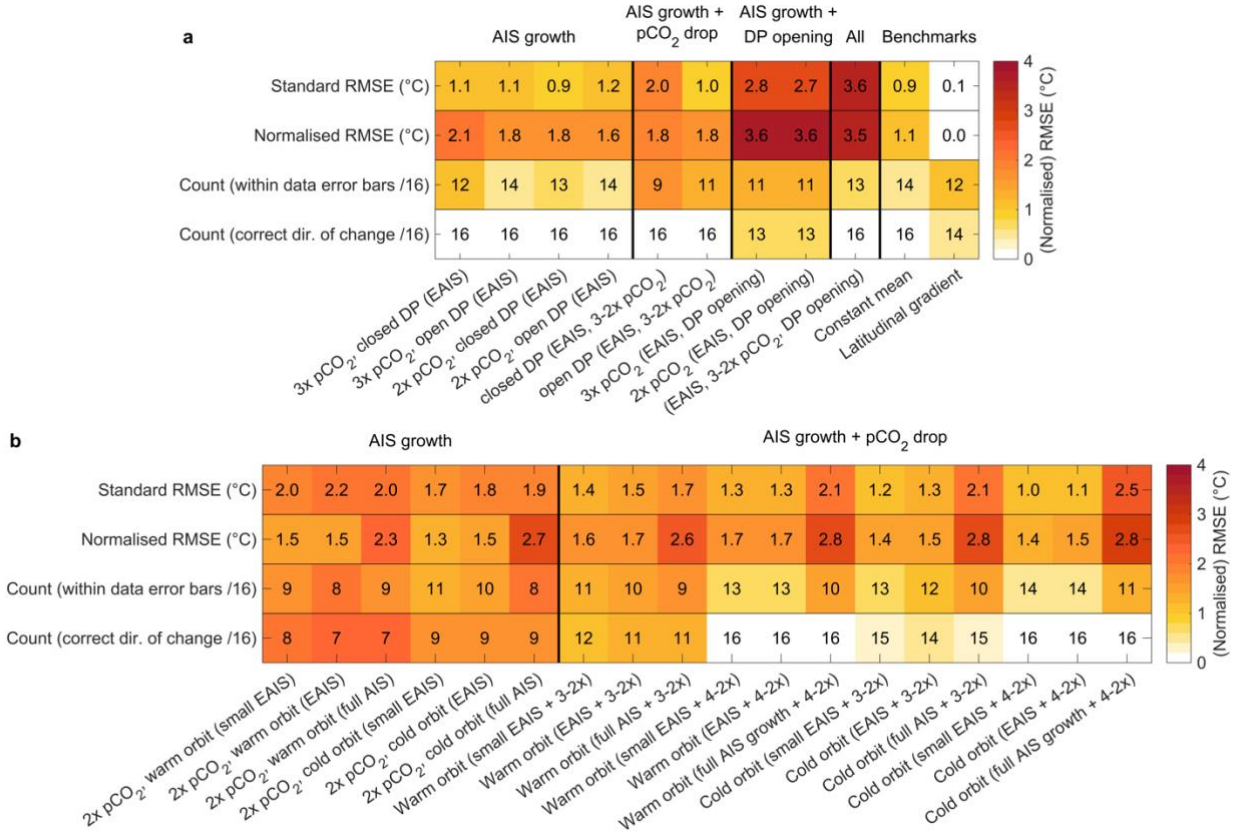

Supplementary Figure 3: Standard RMSE (°C), normalised RMSE (°C) and count metrics for the summer (DJF) mean temperature from all pairs of model simulations representing the forcing across the EOT compared against the EOT dataset from HadCM3BL and the benchmarks (a) and FOAM (b). The simulation pairs are grouped by forcing. Labels on the x-axis are similar to Supplementary Figure 2, with changes in boundary conditions associated with each pair of simulations written in brackets. The colour scales of the count metrics are normalised to match that of the RMSE metrics and stars indicate *moderate*/*good* performance as in Supplementary Figure 2.

References

Birkenmajer, K. & Zastawniak, E.: Late Cretaceous–Early Tertiary floras of King George Island, West Antarctica: their stratigraphic distribution and palaeoclimatic significance, In: Crame, J.A. (Ed.), Origins and Evolution of the Antarctic Biota, Geological Society Special Publication 147, pp. 227–240, 1989.

Bohaty, S.M., Zachos, J.C. & Delaney, M.L.: Foraminiferal Mg/Ca evidence for Southern Ocean cooling across the Eocene-Oligocene transition, *Earth and Planetary Science Letters*, 317-318, pp. 251-261, DOI: 10.1016/j.epsl.2011.11.037, 2012.

Douglas, P.M.J., Affek, H.P., Ivany, L.C., Houben, A.J.P., Sijp, W.P., Sluijs, A., Schouten, S. & Pagani, M.: Pronounced zonal heterogeneity in Eocene southern high-latitude sea surface temperatures, *PNAS*, 111, 18, pp. 6582-6587, DOI: 10.1073/pnas.1321441111, 2014.

Francis, J.S. & Hill, R.S.: Fossil Plants from the Pliocene Sirius Group, Transantarctic Mountains: Evidence for Climate from Growth Rings and Fossil Leaves, *Palaios*, 11, 4, pp. 389-396, 1996.

Francis, J.E., Marenssi, S., Levy, R., Hambrey, M, Thorn, V.T., Mohr, B., Brinkhuis, H., Warnaar, J., Zachos, J.C., Bohaty, S.M., & DeConto, R.M.: From Greenhouse to Icehouse – The Eocene/Oligocene in Antarctica. In: Developments in Earth & Environmental Sciences, 8, F. Florindo and M. Siegert (Editors), DOI 10.1016/S1571-9197(08)00008-6, 2009.

Hartman, J.D., Sangiorgi, F., Salabarnada, A., Peterse, F., Houben, A.J.P., Schouten, S., Brinkhuis, H., Escutia, C. & Bijl, P.K.: Paleoceanography and ice sheet variability offshore Wilkes Land, Antarctica – Part 3: Insights from Oligocene–Miocene TEX_{86}-based sea surface temperature reconstructions, *Climate of the Past*, 14, pp. 1275-1297, DOI: 10.5194/cp-14-1275-2018, 2018.

Houben, A.J.P., Bijl, P.K., Pross, J., Bohaty, S.M., Passchier, S., Stickley, C.E., Röhl, U., Sugisaki, S., Tauxe, L., van de Flierdt, T., Olney, M., Sangiorgi, F., Sluijs, A., Escutia, C., Brinkhuis, H.A. & the Expedition 318 Scientists: Reorganization of Southern Ocean Plankton Ecosystem at the Onset of Antarctic Glaciation, *Science*, 340, pp. 341-344, DOI: 10.1126/science.1223646, 2013.

Houben, A. J. P., Bijl, P. K., Sluijs, A., Schouten, S. & Brinkhuis, H.: Late Eocene Southern Ocean cooling and invigoration of circulation preconditioned Antarctica for full-scale glaciation, *Geochemistry, Geophysics, Geosystems*, 20, pp. 2214–2234. DOI: 10.1029/2019GC008182, 2019.

Kennedy-Asser, A.T., Lunt, D.J., Farnsworth, A. & Valdes, P.J: Assessing mechanisms and uncertainty in modelled climatic change at the Eocene-Oligocene Transition, *Paleoceanography and Paleoclimatology*, 34, pp. 16-34, DOI: 10.1029/2018PA003380, 2019.

Kennedy-Asser, A. T.: EOT_SOcean (accessed 29th August 2019), https://doi.org/10.17605/OSF.IO/BKN26, 2019.

Korasidis, V.A., Wallace, M.W., Wagstaff, B.E. & Hill, R.S.: Terrestrial cooling record through the Eocene-Oligocene transition of Australia, *Global and Planetary Change*, 173, pp. 61-72, DOI: 10.1016/j.gloplacha.2018.12.007, 2019.

Ladant, J.B., Donnadieu, Y., Lefebvre, V. & Dumas, C.: The respective role of atmospheric carbon dioxide and orbital parameters on ice sheet evolution at the Eocene-Oligocene transition, *Paleoceanography*, DOI: 10.1002/2013PA002593, 2014.

Liu, Z., Pagani, M., Zinniker, D., DeConto, R., Huber, M., Brinkhuis, H., Shah, S.R., Leckie, R.M., & Pearson, A.: Global cooling during the Eocene–Oligocene climate transition, *Science*, 323, pp. 1187-1190, DOI: 10.1126/science.1166368, 2009.

Passchier, S., Bohaty, S.M., Jiménez-Espejo, F., Pross, J., Röhl, U., van de Flierdt, T., Escutia, C. & Brinkhuis, H.: Early Eocene to middle Miocene cooling and aridification of East Antarctica, *Geochemistry, Geophysics, Geosystems*, 14, 5, pp. 1399-1410, DOI: 10.1002/ggge.20106, 2013.

Passchier, S., Ciarletta, D.J., Miriagos, T.E., Bijl, P.K. & Bohaty, S.M.: An Antarctic stratigraphic record of stepwise ice growth through the Eocene-Oligocene transition, *GSA Bulletin*, DOI: 10.1130/B31482.1, 2016.

Petersen, S.V. & Schrag, D.P.: Antarctic ice growth before and after the Eocene-Oligocene transition: New estimates from clumped isotope paleothermometry, *Paleoceanography*, 30, pp. 1305-1317, DOI: 10.1002/2014PA002769, 2015.

Pound, M.J. & Salzmann, U.: Heterogeneity in global vegetation and terrestrial climate change during the late Eocene to early Oligocene transition, *Scientific Reports*, 7, p. 43386, DOI: 10.1038/srep43386, 2017.

Prebble, J.G., Raine, J.I., Barrett, P.J. & Hannah, M.J.: Vegetation and climate from two Oligocene glacioeustatic sedimentary cycles (31 and 24 Ma) cored by the Cape Roberts Project, Victoria Land Basin, Antarctica, *Palaeogeography, Palaeoclimatology, Palaeoecology*, 231, pp. 41-57, DOI: 10.1016/j.palaeo.2005.07.025, 2006.

Trusswell, E.M. & Macphail, M.K.: Polar forests on the edge of extinction: what does the fossil spore and pollen evidence from East Antarctica say? *Australian Systematic Botany*, 22, pp. 57-106, DOI: 10.1071/SB08046, 2009.

Villa, G., Fioroni, C., Persico, D., Roberts, A.P. & Florindo, F.: Middle Eocene to Late Oligocene Antarctic glaciation/deglaciation and Southern Ocean productivity, *Paleoceanography*, 29, pp. 223-237, DOI: 10.1002/2013PA002518, 2013.

Zonneveld, K.A.F., Marret, F., Versteegh, G.J.M., Bogus, K., Bonnet, S., Bouimetarhan, I., Crouch, E., de Vernal, A., Elshanawany, R., Edwards, L., Esper, O., Forke, S., Grøsfjeld, K., Henry, M., Holzwarth, U., Kielt, J.F., Kim, S.Y., Ladouceur, S., Ledu, D., Chen, L., Limoges, A., Londeix, L., Lu, S.H., Mahmoud, M.S., Marino, G., Matsouka, K., Matthiessen, J., Mildenhal, D.C., Mudie, P., Neil, H.L., Pospelova, V., Qi, Y., Radi, T., Richerol, T., Rochon, A., Sangiorgi, F., Solignac, S., Turon, J.L., Verleye, T., Wang, Y., Wang, Z. & Young, M.: Atlas of modern dinoflagellate cyst distribution based on 2405 data points, *Review of Palaeobotany and Palynology*, 191, pp. 1-197, DOI: 10.1016/j.revpalbo.2012.08.003, 2013.